NANO LETTERS

Letter

pubs.acs.org/NanoLett

Control of Plasmon Emission and Dynamics at the Transition from Classical to Quantum Coupling

Vasily Kravtsov,[†] Samuel Berweger,[‡] Joanna M. Atkin,[†] and Markus B. Raschke*[,†]

[†]Department of Physics, Department of Chemistry, and JILA, University of Colorado, Boulder, Colorado 80309, United States

[‡]National Institute of Standards and Technology, Boulder, Colorado 80305, United States

ABSTRACT: With nanosecond radiative lifetimes, quenching dominates over enhancement for conventional fluorescence emitters near metal interfaces. We explore the fundamentally distinct behavior of photoluminescence (PL) with few-femtosecond radiative lifetimes of a coupled plasmonic emitter. Controlling the emitter−surface distance with subnanometer precision by combining atomic force and scanning tunneling distance control, we explore the unique behavior of plasmon dynamics at the transition from long-range classical resonant energy transfer to quantum coupling. Because of the ultrafast radiative plasmon emission, classical quenching is completely suppressed. Field-enhanced behavior dominates until the onset of quantum coupling dramatically reduces emission intensity and field enhancement, as verified in concomitant tip-enhanced Raman measurements. The entire distance behavior from tens of nanometers to subnanometers can be described using a phenomenological rate equation model and highlights the new degrees of freedom in radiation control enabled by an ultrafast radiative emitter near surfaces.

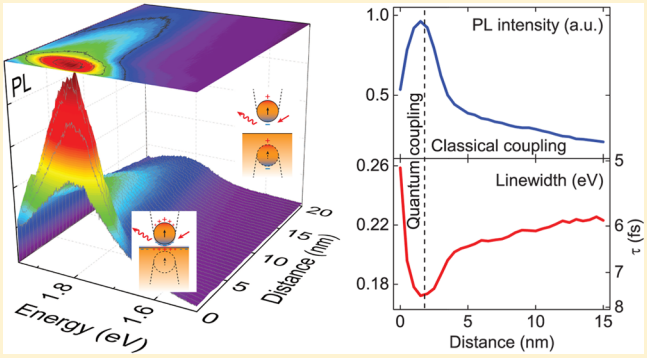

KEYWORDS: *Plasmonic emitter, photoluminescence, quantum coupling, tunneling, radiative lifetime*

The coupling of a classical or quantum emitter to another emitter or to an interface can profoundly modify the lifetime, quantum yield, and radiation pattern of the emission.[1−5] In particular for photoluminescence (PL) of atoms, molecules, or quantum dots near a metal surface or nanostructure, the dependence of the radiation on the emitter−metal distance is determined by the competition between enhancement due to changes in local electromagnetic density of states and quenching due to near-field coupling and fast nonradiative damping through energy dissipation into the substrate.[6,7] For typical fluorescent emitters with free-space radiative lifetimes in the few nanosecond regime, quenching dominates for distances shorter than ∼10 nm, due to the ultrafast inelastic Drude damping in the 10−30 fs range in the metal. This limits the degrees of freedom for radiation control, desirable for a wide range of fundamental and technological applications.[8]

Here we explore a distinctly different regime of emitter-substrate coupling based on the photoluminescence (PL) of a plasmonic emitter. With its mesoscopic dimensions exceeding those of molecules and quantum dots and the associated antenna effect, the plasmonic emitter exhibits *femtosecond* as opposed to nanosecond radiative lifetimes.[9−12] This allows the plasmonic emitter to compete more favorably against the fast inelastic Drude damping of the coupled metal substrate.

We take advantage of the precise distance control of shear-force atomic force microscopy (AFM) combined with scanning tunneling microscopy (STM) to measure distance-dependent intensity, spectral shift, and lifetime of the PL of the apex of plasmonic tips near a metal surface. We find that the PL is enhanced for all distances of classical near-field coupling, with increasing lifetime, and only quenched at the subnanometer length range, with associated rapid decrease in lifetime, due to nonlocal or tunneling charge transfer quantum effects. The entire distance-dependent behavior can be modeled by coupled rate equations for the optical excitation, including near-field resonant energy transfer (RET) and nonradiative energy dissipation. Concurrent distance dependent tip-enhanced Raman spectroscopy (TERS) measurements are found to be in excellent agreement with the predicted behavior based on the same parameter set, including the associated reduced field-enhancement in the quantum coupling regime.

The PL of plasmonic emitters has recently been identified as a useful tool for the study of the underlying plasmon resonances in single and coupled nanostructures.[13−16] As shown for Au nanorods, the PL spectrum reflects the plasmon resonance of the nanoparticle.[17,18] The broad line width is a measure of the intrinsically short dephasing times, resulting in very short radiative plasmon-coupled PL lifetimes.[9,11]

Much recent interest has been devoted to how quantum effects modify the plasmon resonance of coupled systems at small interparticle separations.[19−22] Deviations from the

Received: June 19, 2014
Revised: July 28, 2014
Published: August 4, 2014

   dx.doi.org/10.1021/nl502297t | *Nano Lett.* 2014, 14, 5270−5275

classical prediction for spectral shift and near-field enhancement have been observed for distances smaller than 0.3−1.0 nm and attributed to quantum effects.[23−27] However, questions remain as to the relative role of nonlocality or quantum tunneling[22,23,25,28] associated in part with the difficulties of precise subnanometer distance control. Our work extends these studies, with precise ∼0.3 nm distance control showing how quantum effects modify the plasmon lifetime and emission intensity of the coupled plasmon excitation for an individual nanostructure in a reproducible way.

The experimental layout is shown in Figure 1a. The Au sample is prepared by template stripping a thermally evaporated 100 nm thick Au layer on a Si wafer[29] (surface roughness ≲0.3 nm). Gold tips (inset, SEM image) are etched electrochemically,[30] with ∼10−20 nm apex radius. They are mounted to a quartz tuning fork with lateral dither piezo excitation (D) for shear-force tip−sample distance control.[31] The tip can simultaneously be biased for STM measurements.[32] The tip−sample distance is controlled by a calibrated piezo stage (Physik Instrumente). Both shear-force AFM and STM circuit are operated by a digital AFM controller (RHK Technology, R9).

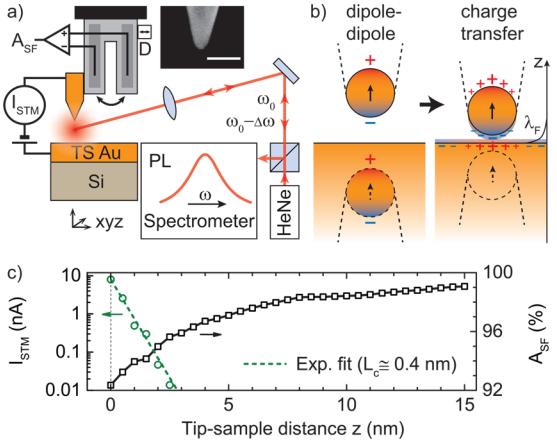

Figure 1. (a) Schematic of experimental setup, with SEM image of tip apex (scale bar 100 nm). Tip−sample distance controlled with shear-force AFM and calibrated with STM. The surface plasmon and PL of tip apex are excited by a 632.8 nm HeNe laser and detected spectroscopically in backscattering geometry. (b) Classical and quantum coupling regime for distances larger (left) or less than the tunneling range (with Fermi wavelength λ_F) (right). (c) Distance dependence of shear-force amplitude A_{SF} (black squares, line is a guide for the eye) and tunneling current I_{STM} (green circles), with an exponential fit (green dashed line).

Figure 1b shows a schematic of the optical coupling between the plasmonic tip apex and the flat gold surface for both the classical dipole (left) and the quantum coupling regime (right). Figure 1c shows the simultaneously measured tip−sample distance dependence of tunneling current I_{STM} and shear-force amplitude A_{SF}. The onset of shear-force at $z \sim$ 10−20 nm and tunneling at $z <$ 2 nm for bias voltage of 100 mV is typical room temperature behavior under ambient conditions at moderate relative humidity.[32,33] The shear-force feedback loop provides 0.3 nm z-position accuracy over a wide distance range. In contrast, STM, with 0.1 nm accuracy and the much steeper and well defined tunneling distance dependence, provides for accurate short distances control and definition of zero tip-sample distance.[32] We define zero distance at 10 nA tunneling current, corresponding to a tip−surface separation of one Au van der Waals diameter (∼0.33 nm). We estimate the overall absolute distance accuracy as 0.3 nm, possibly limited by electrostatic forces modifying the tip shape on the atomic scale.

A HeNe laser (632.8 nm, 1.96 eV) is focused onto the tip apex with an objective lens (NA = 0.5, Olympus) in side illumination, at 1 mW power, polarized along the tip axis. The signal is collected in back scattering, directed through a long pass 633 nm edge filter, and detected with a grating spectrometer coupled to a LN_2-cooled CCD camera (Princeton Instruments). The signal is linear in incident power and is attributed to PL, as in previous reports.[13−15,17,18] The total collection efficiency of the setup is estimated as ∼5%. We ensure complete equilibration of the tuning fork probe head in order to eliminate any thermal drifts and instabilities caused by the incident laser beam.

Figure 2a shows the spectral evolution of the PL with distance measured in 0.5 nm increments and 0.5 s acquisition time per spectrum. While spectral details vary from tip to tip, a

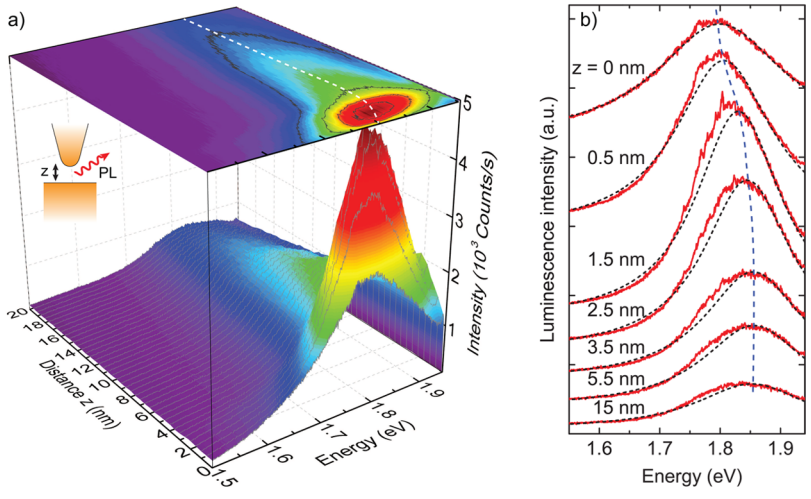

Figure 2. (a) Evolution of Au tip PL spectra as a function of distance to the Au-surface, z. Pronounced field-enhancement is followed by rapid quenching for $z <$ 2 nm. The dashed white line in the 2D projection shows the associated spectral peak shift. (b) Representative PL spectra (red, solid) for selected tip−sample distances (offset for clarity) with Lorentzian fits (black, dashed).

dx.doi.org/10.1021/nl502297t | Nano Lett. 2014, 14, 5270−5275

single peak with center frequency in the 1.7−1.9 eV range, with full width at half-maximum (fwhm) of 0.2−0.3 eV, is observed for most tips. The PL signal is predominantly polarized parallel to the tip axis (p), with >10 contrast between p and s polarization. This behavior is in good general agreement with previous measurements of plasmonic Au tip PL,[13,30] near-field tip-scattering,[34] and femtosecond time-resolved spectroscopy.[35] Control experiments performing the same measurements on the sample in the absence of the tip show a negligible, at least 2 orders of magnitude weaker, PL signal.

PL in metals originates from radiative interband recombination of d-band holes and sp-band electrons and is usually weak due to competing fast nonradiative electron−electron and electron−phonon scattering.[36] Plasmonic enhancement can resonantly increase the PL response[37,38] and allow for intraband transitions due to large momenta associated with surface plasmons (SP).[39] The spectral shape of the PL reflects the plasmon resonance,[17,18,40] and thus the measured distance dependence reflects the coupled plasmon dynamics.[13]

From the PL spectra, three distinct distance regimes of PL intensity and spectral evolution can be identified: (i) an initial long-range moderate intensity increase due to far-field interference with little spectral change is followed by (ii) a pronounced near-field signal increase and spectral redshift below $z \sim 5$ nm and (iii) a regime of quenching and significant line broadening at $z \lesssim 1.5$ nm. This behavior is generally reproducible in repeated approach and retraction experiments.

The tunneling current does not influence intensity and spectral behavior due to low bias voltage, which is verified from comparison of tunneling vs shear force approach. This is in contrast to experiments on emission from metals and molecules,[41,42] where a PL contribution has been shown to originate from excitation by tunneling electrons.

We perform a detailed Lorentzian line shape analysis of the spectra from Figure 2a, as shown in Figure 2b for a representative set of spectra for different distances. The spectral features omitted from analysis in the narrow range from 1.75 to 1.82 eV are due to TERS from residual surface and tip contamination of carbonaceous material.[43,44] The derived intensity I, peak position ω_0, and fwhm Γ are plotted in Figure 3a−c as functions of tip−sample distance. The error bars shown represent the uncertainty in reproducibility of repeated measurements. The first distinct feature is the continuous enhancement of the PL (a, circles) with decreasing distance well into the few nanometer range—a regime which for a molecular emitter near a metal surface is characterized by strong quenching due to resonant energy transfer. The continuous spectral red shift (b) is due to the softening of the coupled plasmon response,[45] and associated slight spectral narrowing (c) is due to the decreasing influence of interband damping.[11] Concomitant with the onset of tunneling for $z \lesssim 1.5$ nm (a−c, green dashed line), a turnover is observed with decreasing intensity and significant line broadening due to additional nonradiative dissipation in the quantum coupling regime.

In the following we will separately discuss the different distance regimes observed where intensity, resonant frequency, and plasmon damping behavior reveal the distinct length scales of the underlying coupling mechanisms. For distances larger than the tip apex radius, slight variations in intensity and line width are due to far-field interference modulation of the emission similar to the behavior observed in atomic or molecular fluorescence near a metal surface.[1,6,16,46] When the

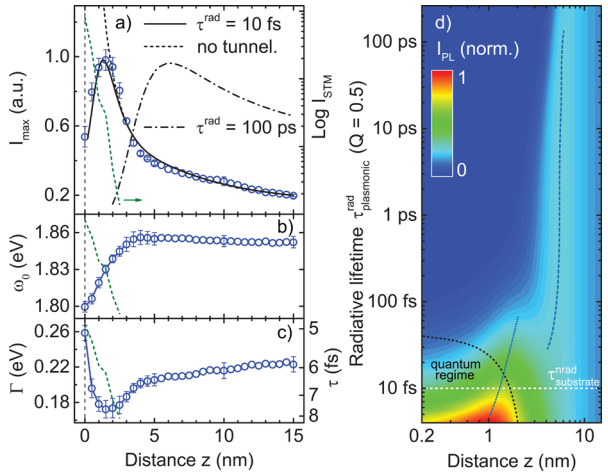

Figure 3. Distance dependence of tip plasmon PL intensity I (a, circles), peak position (b), and line width (c). Simulated PL intensity for 10 fs emitter with (solid black) and without (dashed black) tunneling term using the model described in the text. For comparison, simulated PL intensity for 100 ps emitter (dash-dotted). Tunneling current I_{STM} (green dashed line) for reference. In (b) and (c) solid lines are guides for the eye, and scale for tunneling curve is omitted. (d) Simulated distance dependence of normalized PL intensity as function of radiative lifetime, for fixed quantum efficiency of $Q = 0.5$ and $\tau^{nrad}_{substrate} = 10$ fs as example. This illustrates the transition of peaked intensity from classical and long-range damped regime (blue, dashed) to the ultrafast radiative and quantum coupling regime (blue, dotted).

tip−sample distance becomes comparable to the tip apex radius ($z \simeq R \lesssim 10$ nm), near-field enhancement in the tip−sample gap increases both the excitation laser field intensity and PL plasmon polarization.[11] This gives rise to an increase in emitted PL intensity due to the small intrinsic quantum yield of plasmon PL (Figure 3a). In addition, the SP resonance softens and red shifts for the radiative bonding plasmon mode, due to Coulomb interaction between opposite charges on the surface of the tip apex and substrate[45] (Figure 3b). The plasmon line width (Figure 3c) of $\Gamma_{SP} = 0.22$ eV for long distances (corresponding to $\tau = 2\hbar/\Gamma = 6$ fs) has both radiative Γ^{rad} and nonradiative Γ^{nrad} contributions. $\Gamma^{nrad} \simeq 0.10$ eV ($\tau^{nrad} \simeq 13-14$ fs) at $\omega_0 \simeq 1.8$ eV, estimated from a quasi-static model,[11] is composed of Drude relaxation $\Gamma^{Drude} \simeq 0.07$ eV ($\tau^{Drude} \simeq 18$ fs) and interband damping $\Gamma^{inter} \simeq 0.03$ eV ($\tau^{inter} \simeq 50$ fs). With increasing redshift the interband damping decreases, and the observed 0.05 eV redshift is in good agreement with a 0.03 eV decrease in line width, corresponding to a ∼1 fs decrease in nonradiative lifetime.[9,11]

Radiative lifetimes in the few femtosecond range for spherical plasmonic particles in the few tens of nanometers size range can be derived using Mie theory.[11] From our experimental results we estimate $\Gamma^{rad} = \Gamma_{SP} - \Gamma^{nrad} \simeq 0.12$ eV, corresponding to $\tau^{rad} \simeq 10$ fs.

The radiative lifetime of a classical oscillating dipole scales with frequency as $\tau_{rad} \propto \omega_0^{-2}$. Therefore, the redshift of the plasmon resonance for decreasing tip−sample distance would lead to longer radiative lifetimes, as observed. This also agrees with recent simulations of the plasmon resonance of a dimer,[47,48] where the radiative damping rate decreases for smaller interparticle distances. However, for the observed 0.05 eV redshift, this effect is not expected to contribute significantly and would only result in a <10% increase in the radiative lifetime.

dx.doi.org/10.1021/nl502297t | Nano Lett. 2014, 14, 5270−5275

For distances $z \lesssim 1.5$ nm, and independent of tip radius and near-field coupling, the PL quenching and decrease in SP lifetime is found to correlate with the onset of dc tunneling (Figure 3a, green dashed line). To describe the crossover from classical near-field coupling to quantum coupling, we introduce an empirical rate equation model for the time and distance dependence of the electromagnetic energy for the tip P_{tip} and sample P_s:

$$\frac{dP_{tip}}{dt} = \Gamma_e(z) - (\Gamma_{tip} + \Gamma_d(z) + \Gamma_{RET}(z))P_{tip} + \Gamma_{RET}(z)P_s$$

$$\frac{dP_s}{dt} = -(\Gamma_s + \Gamma_d(z) + \Gamma_{RET}(z))P_s + \Gamma_{RET}(z)P_{tip}$$

Here, $\Gamma_e(z) \propto (1 - \kappa\alpha(\epsilon_{Au} - 1)/16\pi(\epsilon_{Au} + 1)(R + z)^3)^{-2}$ describes the distance-dependent excitation rate in the coupled dipole approximation, with the tip apex represented by a sphere of radius R and polarizability $\alpha = 4\pi R^3(\epsilon_{Au} - 1)/(\epsilon_{Au} + 2)$, where ϵ_{Au} is the dielectric constant of gold at $\omega_0 \simeq 1.8$ eV. The free parameter κ accounts for possible deviation from the ideal spherical shape. Radiative and nonradiative damping rates are considered for the tip $\Gamma_{tip} = \Gamma_{tip}^{rad} + \Gamma_{tip}^{nrad}$, and purely nonradiative contributions for the substrate Γ_s^{nrad}. Furthermore, we describe the nonradiative resonance energy transfer (RET) rate as $\Gamma_{RET}(z) = \Gamma_{tip}^{rad}(R_0/z)^m$, with $m = 4$ due to the reduced dimensionality, and the characteristic length scale of near-field energy transfer R_0.[49] We introduce additional energy dissipation due to quantum effects assumed to scale as $\Gamma_d(z) \propto \exp(-z/l_c)$ as a nonradiative, bidirectional decay channel. We then solve the coupled differential equations for $P^0_{tip}(z)$ in steady state, in order to obtain the PL intensity $I_{PL}(z) \propto \Gamma_{tip}^{rad}P^0_{tip}(z)$.

The experimental conditions can be described using $\Gamma_{tip}^{rad} \simeq \Gamma_{tip}^{nrad} \simeq \Gamma_s^{nrad} \simeq 0.1$ eV from above. From the fit of the coupled differential equations to the results in Figure 3a we then obtain $R_0 = 5 \pm 2$ nm for the near-field energy transfer $\Gamma_{RET}(z)$. This value is in agreement with characteristic length for an oscillating dipole near a metal interface $R_0 = (0.255c^3Q/\omega_0^2\omega_F k_F)^{1/4} \simeq 4$ to 12 nm, with intrinsic quantum yield $Q = 0.01...1$, resonant energy $\omega = 1.8$ eV, Fermi frequency ω_F, and wave vector k_F of the metal.[50] For the quantum coupling regime we find $l_c = 0.4 \pm 0.1$ nm, in good agreement with the characteristic distance of $L_c \simeq 0.42 \pm 0.04$ nm obtained by exponential fitting of the tunneling current.

Together with tip radius $R = 25 \pm 5$ nm and $\kappa = 2.4 \pm 0.1$, the model provides an excellent fit of the entire distance dependence range as seen in Figure 3a (solid black line). Neglecting quantum effects, yet for otherwise identical parameters, the PL would continue to rise (dashed black), with the field-enhancement outcompeting the RET quenching for all distances.

To show how the distance dependence for the plasmonic emitter with femtosecond radiative lifetimes is qualitatively different compared to a molecular emitter, Figure 3a shows the results for a hypothetical case of $\tau_{tip}^{rad} = 100$ ps (dashed−dotted line). Here, with the large unfavorable ratio of $\tau_{tip}^{rad}/\tau_s^{nrad} \sim 10^4...10^5$ the PL is quenched effectively by nonradiative energy transfer below a distance of ∼6 nm, in agreement with the distance range of corresponding experimental results of atomic/molecular emitters.[7,50]

The general effect of the radiative lifetime on the PL quenching behavior is illustrated in Figure 3d, where we model the distance dependence of PL for emitters with different radiative times, for a fixed arbitrary quantum yield $\Gamma^{rad}/(\Gamma^{rad} + \Gamma^{nrad}) = 0.5$. It can be seen that for molecular emitters (hundreds of picoseconds to nanoseconds lifetimes) PL is quenched below 5−10 nm. However, as the lifetime of an emitter approaches the inelastic relaxation times of the metal of $\tau^{nrad} \sim 10$ fs (white dashed line), radiative emission becomes increasingly favorable. In addition, femtosecond emission is continuously enhanced throughout the entire classical coupling regime, and only limited at subnanometer distances where quantum effects trigger the decay of plasmon coherence into single particle excitation.

The quenching of PL due to quantum effects has implications for plasmon-enhanced molecular spectroscopies. In the following we analyze the effect of quantum coupling on the field enhancement in TERS. Figure 4 shows the

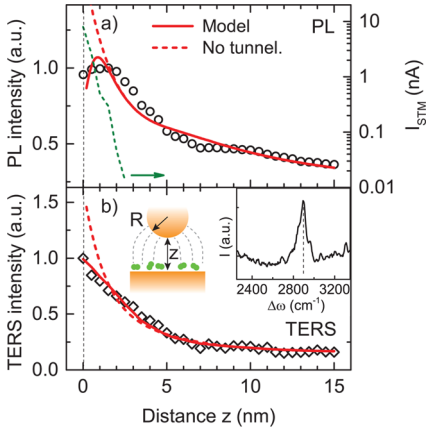

Figure 4. (a) Distance dependence of PL intensity: experimental data (circles) and simulation with (red solid line) and without (red dashed) energy dissipation due to quantum effects for coupled plasmonic tip−sample system; measured dc tunneling current (green dashed). (b) TERS signal for the C−H stretch vibrational mode (inset, spectrum) of the residual surface molecules: experimental data (rhombs), simulation with (red solid line) and without (red dashed) tunneling shows the field-enhancement limited by quantum coupling.

simultaneous acquisition of PL (a, circles) and TERS for a $\Delta\omega = 2900$ cm^{-1} C−H stretch vibrational mode of surface hydrocarbons (b, diamonds) that are intrinsically present in small amounts on the sample under the ambient experimental conditions. The model PL fit with (red solid) and without (red dashed) the quantum contribution $\Gamma_d(z)$ is obtained for similar fit parameters as for the data shown in Figure 3a, except for a different tip radius $R = 40 \pm 5$ nm and $\kappa = 2.0 \pm 0.1$ (data in Figure 3 and Figure 4 were taken with different tips).

We take into account equal plasmonic field enhancement $\mathcal{F}$ for both excitation and emission of both PL and TERS. However, the TERS intensity of the induced radiative tip polarization from the molecular emitter located at the metal surface scales differently compared to PL with the emitter located in the tip apex. Starting with a single molecular TERS emitter with dipole moment p at the surface, the tip-induced and -scattered Raman emission $I_{TERS} \propto (\mathcal{F}p)^4(1/(R + z)^3)^4$. Then integrating I_{TERS} over the surface projected area under the tip gives rise to an approximate relation $I_{TERS} \propto I_{PL}/(R + z)^{10}$. Applying this scaling to the experimental PL data predicts a *continuously* rising TERS intensity (b, red solid) over the entire distance regime, in good agreement with the experiment (diamonds). This corresponds to the fact that with its near *instantaneous* response the Raman signal is not effectively

dx.doi.org/10.1021/nl502297t | *Nano Lett.* 2014, 14, 5270−5275

quenched, neither by RET nor by quantum effects. However, as evident when calculating the TERS intensity from PL without quantum effects (red dashed line), the TERS intensity is reduced in the quantum coupling regime. This is due to a decrease in field-enhancement caused by quantum effects, thus suppressing the otherwise rapid TERS signal rise expected from the z^{-10} scaling. These results are in agreement with predictions and recent findings of reduced field enhancement in antenna structures for surface-enhanced Raman scattering with the onset of charge transfer.[51,52]

Due to the femtosecond radiative lifetimes for plasmonic emitters, the results presented above allow for the distinction of short-range quantum effects, which are typically obscured for molecular emitters by classical quenching. The deviations of coupled plasmon resonators from classical predictions at short distances have recently been discussed in terms of nonlocal dielectric effects or quantum tunneling. For example, based on a full quantum treatment of a plasmonic dimer, deviations from classical behavior of plasmon resonance and field enhancement at interparticle distances of <1 nm were attributed to quantum tunneling.[20] While recent experiments are consistent with the predicted behavior,[24−27] nonlocality of the metal dielectric response has been suggested as an alternative mechanism.[22,23] The characteristic length scales for both tunneling (Fermi wavelength λ_F) and nonlocal effects (convection length $l_C = v_F/\omega_0$ with Fermi velocity v_F) can be estimated for Au as ∼0.5 nm. Thus, with both effects being of quantum nature and exhibiting similar length scaling their experimental distinction is difficult in principle. Despite the increased accuracy and precision in distance control in our experiment, as well as the overall increase in parameter space with measurement of intensity and spectral evolution including the independent TERS-based field enhancement, we are not able to discriminate between the two proposed models. Future experiments in this direction can investigate plasmonic coupling either for different materials, where the ratio of nonlocal and tunneling characteristic distances varies due to differences in Fermi energy, or for structures with the length scale of nonlocal effects varying through the frequency of the plasmon resonance.

In summary, the distance dependence of the PL response of a coupled plasmonic structure analyzed in this work demonstrates that classical quenching becomes inefficient for the case of a plasmonic emitter, where the femtosecond radiative lifetime of the emitter competes favorably against the 10−30 fs inelastic Drude damping. The use of shorter radiative lifetimes and/or substrates with longer nonradiative decay times could therefore greatly extend the range of radiation control through both classical as well as quantum emitter to substrate coupling.

AUTHOR INFORMATION

Corresponding Author

*E-mail: markus.raschke@colorado.edu.

Notes

The authors declare no competing financial interest.

ACKNOWLEDGMENTS

We would like to acknowledge funding from the Department of Energy Division of Materials Sciences and Engineering (Grant No. DE-SC0002197) and the National Science Foundation (NSF grant No. CHE1306398).

REFERENCES

(1) Drexhage, K. H. *J. Lumin.* **1970**, *1*, 693−701.
(2) Drexhage, K. H. *Prog. Opt. Commun.* **1974**, *12*, 163−232.
(3) Ford, G. W.; Weber, W. H. *Phys. Rep.* **1984**, *113*, 195−287.
(4) Ming, T.; Chen, H.; Jiang, R.; Li, Q.; Wang, J. *J. Phys. Chem. Lett.* **2012**, *3*, 191−202.
(5) Tan, S. F.; Wu, L.; Yang, J. K.; Bai, P.; Bosman, M.; Nijhuis, C. A. *Science* **2014**, *343*, 1496−1499.
(6) Buchler, B. C.; Kalkbrenner, T.; Hettich, C.; Sandoghdar, V. *Phys. Rev. Lett.* **2005**, *95*, 063003.
(7) Anger, P.; Bharadwaj, P.; Novotny, L. *Phys. Rev. Lett.* **2006**, *96*, 113002.
(8) Lakowicz, J. R. *Anal. Biochem.* **2005**, *337*, 171−194.
(9) Sonnichsen, C.; Franzl, T.; Wilk, T.; von Plessen, G.; Feldmann, J.; Wilson, O.; Mulvaney, P. *Phys. Rev. Lett.* **2002**, *88*, 077402.
(10) Hanke, T.; Cesar, J.; Knittel, V.; Trugler, A.; Hohenester, U.; Leitenstorfer, A.; Bratschitsch, R. *Nano Lett.* **2012**, *12*, 992−996.
(11) Raschke, M. B.; Berweger, S.; Atkin, J. M. In *Plasmonics: Theory and applications*; Shahbazyan, T. V., Stockman, M. I., Eds.; Springer: New York, 2013; Chapter 7, pp 237−281.
(12) Olmon, R.; Raschke, M. *Nanotechnology* **2012**, *23*, 444001.
(13) Pettinger, B.; Domke, K. F.; Zhang, D.; Schuster, R.; Ertl, G. *Phys. Rev. B* **2007**, *76*, 113409.
(14) Sackrow, M.; Stanciu, C.; Lieb, M. A.; Meixner, A. J. *ChemPhysChem* **2008**, *9*, 316−320.
(15) Steiner, M.; Debus, C.; Failla, A. V.; Meixner, A. J. *J. Phys. Chem. C* **2008**, *112*, 3103−3108.
(16) Hakanson, U.; Agio, M.; Kuhn, S.; Rogobete, L.; Kalkbrenner, T.; Sandoghdar, V. *Phys. Rev. B* **2008**, *77*, 155408.
(17) Yorulmaz, M.; Khatua, S.; Zijlstra, P.; Gaiduk, A.; Orrit, M. *Nano Lett.* **2012**, *12*, 4385−4391.
(18) Fang, Y.; Chang, W. S.; Willingham, B.; Swanglap, P.; Dominguez-Medina, S.; Link, S. *ACS Nano* **2012**, *6*, 7177−7184.
(19) Tame, M. S.; McEnery, K. R.; Ozdemir, S. K.; Lee, J.; Maier, S. A.; Kim, M. S. *Nat. Phys.* **2013**, *9*, 329−340.
(20) Zuloaga, J.; Prodan, E.; Nordlander, P. *Nano Lett.* **2009**, *9*, 887−891.
(21) Esteban, R.; Borisov, A. G.; Nordlander, P.; Aizpurua, J. *Nat. Commun.* **2012**, *3*, 825.
(22) Mortensen, N. A.; Raza, S.; Wubs, M.; Sondergaard, T.; Bozhevolnyi, S. I. *Nat. Commun.* **2014**, *5*, 3809.
(23) Ciraci, C.; Hill, R. T.; Mock, J. J.; Urzhumov, Y.; Fernandez-Dominguez, A. I.; Maier, S. A.; Pendry, J. B.; Chilkoti, A.; Smith, D. R. *Science* **2012**, *337*, 1072−1074.
(24) Savage, K. J.; Hawkeye, M. M.; Esteban, R.; Borisov, A. G.; Aizpurua, J.; Baumberg, J. J. *Nature* **2012**, *491*, 574−577.
(25) Scholl, J. A.; Garcia-Etxarri, A.; Koh, A. L.; Dionne, J. A. *Nano Lett.* **2013**, *13*, 564−569.
(26) Mertens, J.; Eiden, A. L.; Sigle, D. O.; Huang, F. M.; Lombardo, A.; Sun, Z. P.; Sundaram, R. S.; Colli, A.; Tserkezis, C.; Aizpurua, J.; Milana, S.; Ferrari, A. C.; Baumberg, J. J. *Nano Lett.* **2013**, *13*, 5033−5038.
(27) Kadkhodazadeh, S.; Wagner, J. B.; Kneipp, H.; Kneipp, K. *Appl. Phys. Lett.* **2013**, *103*, 083103.
(28) Hajisalem, G.; Min, Q.; Gelfand, R.; Gordon, R. *Opt. Express* **2014**, *22*, 9604−9610.
(29) Vogel, N.; Zieleniecki, J.; Koper, I. *Nanoscale* **2012**, *4*, 3820−3832.
(30) Neacsu, C. C.; Steudle, G. A.; Raschke, M. B. *Appl. Phys. B: Laser Opt.* **2005**, *80*, 295−300.
(31) Raschke, M. B.; Lienau, C. *Appl. Phys. Lett.* **2003**, *83*, 5089−5091.
(32) Karrai, K.; Tiemann, I. *Phys. Rev. B* **2000**, *62*, 13174.
(33) Davy, S.; Spajer, M.; Courjon, D. *Appl. Phys. Lett.* **1998**, *73*, 2594−2596.
(34) Neacsu, C. C.; Dreyer, J.; Behr, N.; Raschke, M. B. *Phys. Rev. B* **2006**, *73*, 193406.
(35) Anderson, A.; Deryckx, K. S.; Xu, X. J. G.; Steinmeyer, G.; Raschke, M. B. *Nano Lett.* **2010**, *10*, 2519−2524.

(36) Mooradian, A. *Phys. Rev. Lett.* **1969**, *22*, 185−187.
(37) Boyd, G. T.; Yu, Z. H.; Shen, Y. R. *Phys. Rev. B* **1986**, *33*, 7923−7936.
(38) Mohamed, M. B.; Volkov, V.; Link, S.; El-Sayed, M. A. *Chem. Phys. Lett.* **2000**, *317*, 517−523.
(39) Beversluis, M. R.; Bouhelier, A.; Novotny, L. *Phys. Rev. B* **2003**, *68*, 115433.
(40) Bouhelier, A.; Bachelot, R.; Lerondel, G.; Kostcheev, S.; Royer, P.; Wiederrecht, G. P. *Phys. Rev. Lett.* **2005**, *95*, 267405.
(41) Berndt, R.; Gimzewski, J. K.; Johansson, P. *Phys. Rev. Lett.* **1991**, *67*, 3796−3799.
(42) Rossel, F.; Pivetta, M.; Schneider, W. D. *Surf. Sci. Rep.* **2010**, *65*, 129−144.
(43) Kudelski, A.; Pettinger, B. *Chem. Phys. Lett.* **2000**, *321*, 356−362.
(44) Otto, A. *J. Raman Spectrosc.* **2002**, *33*, 593−598.
(45) Rechberger, W.; Hohenau, A.; Leitner, A.; Krenn, J. R.; Lamprecht, B.; Aussenegg, F. R. *Opt. Commun.* **2003**, *220*, 137−141.
(46) Barnes, W. L. *J. Mod. Opt.* **1998**, *45*, 661−699.
(47) Dahmen, C.; Schmidt, B.; von Plessen, G. *Nano Lett.* **2007**, *7*, 318−322.
(48) Madoyan, K. K.; Melikyan, A. H.; Minassian, H. R. *J. Phys. Chem. C* **2012**, *116*, 16800−16805.
(49) Persson, B. N. J.; Lang, N. D. *Phys. Rev. B* **1982**, *26*, 5409−5415.
(50) Sen, T.; Patra, A. *J. Phys. Chem. C* **2012**, *116*, 17307−17317.
(51) Mao, L.; Li, Z.; Wu, B.; Xu, H. *Appl. Phys. Lett.* **2009**, *94*, 243102.
(52) Halas, N. J.; Lal, S.; Chang, W.; Link, S.; Nordlander, P. *Chem. Rev.* **2011**, *111*, 3913−3961.